Supplementary Information
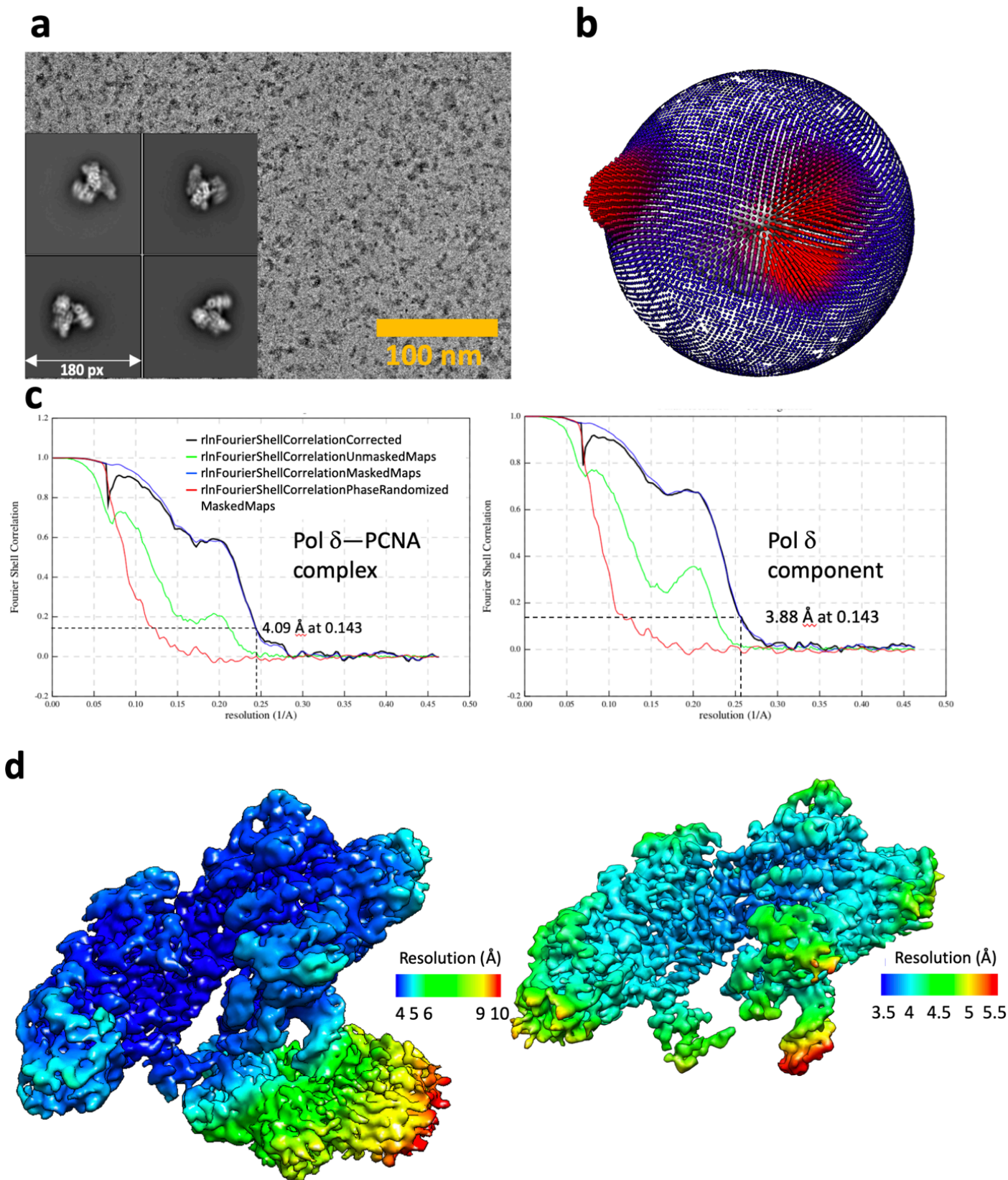
Structure of the processive human Pol δ holoenzyme

Lancey, et al.
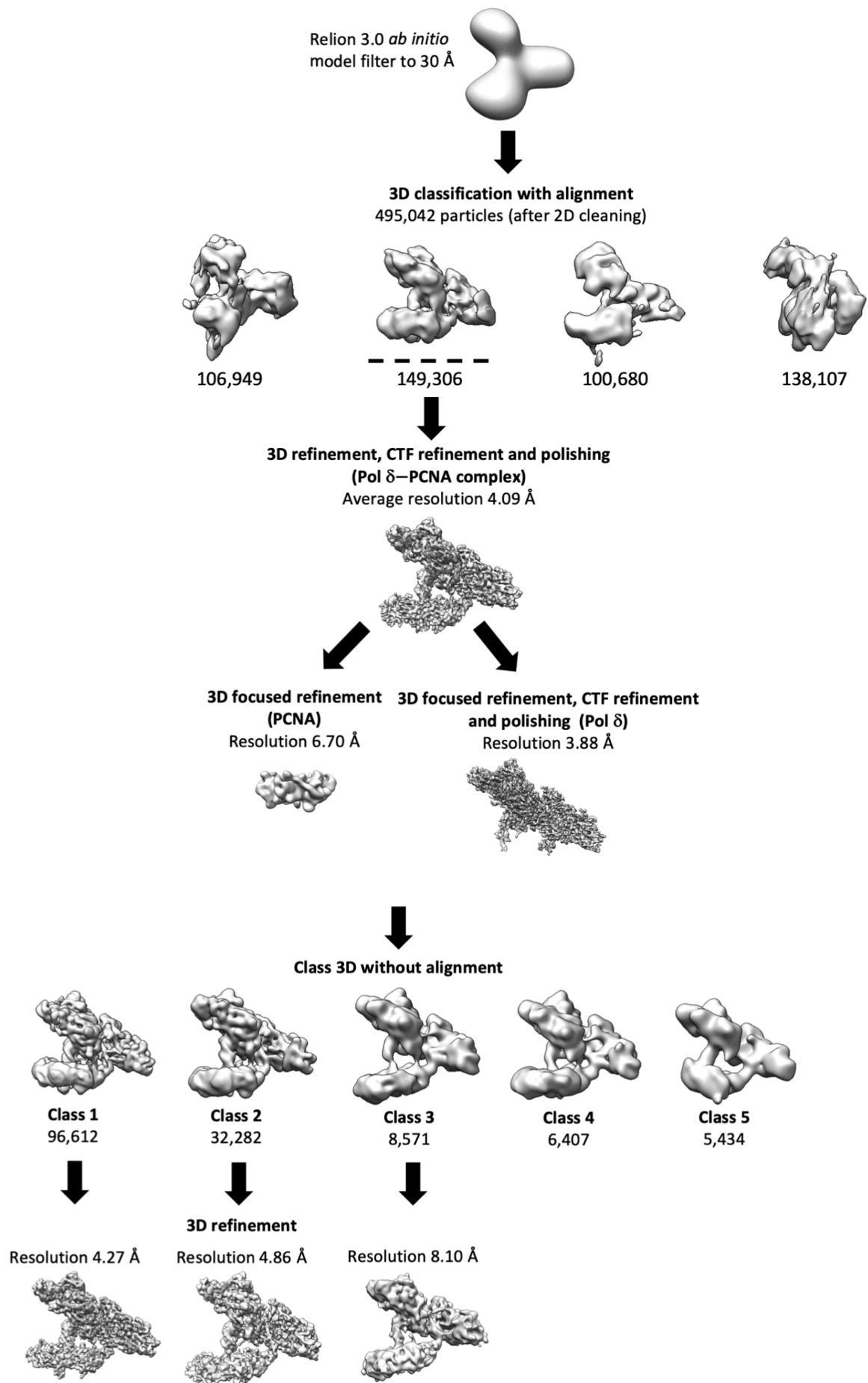
Includes:

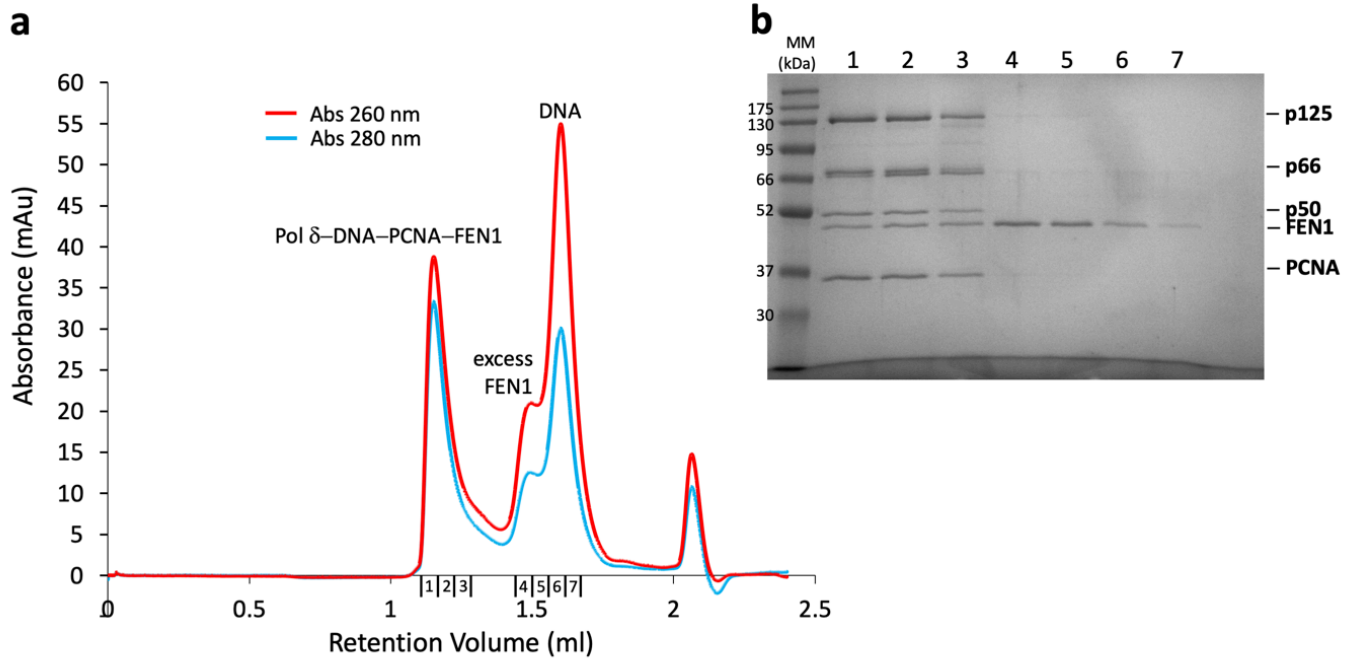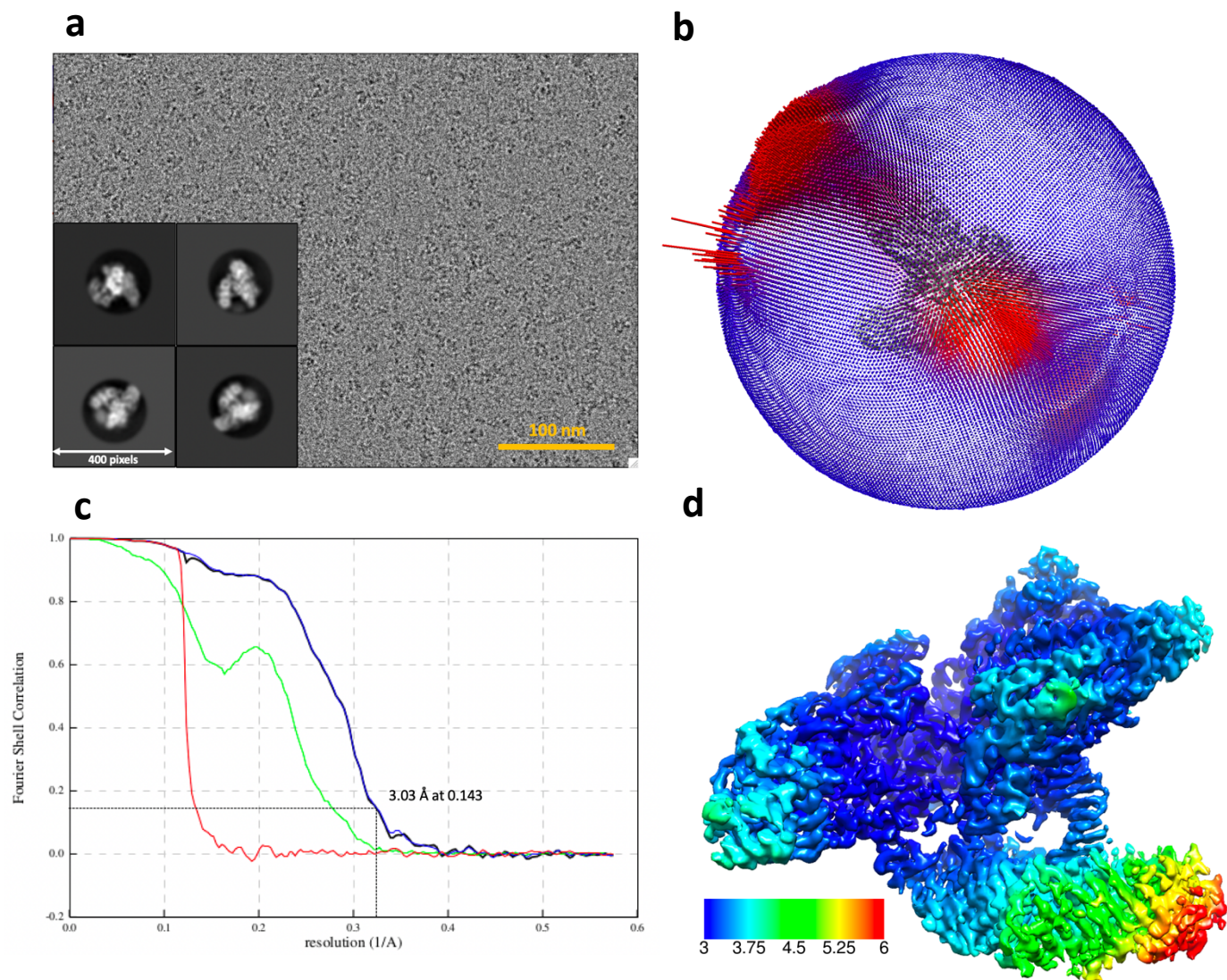**Supplementary Figure 1.** Cryo-EM of the processive Pol δ holoenzyme (Dataset 1). **a)** Electron micrograph (aligned sum) acquired using a Volta phase plate on a Falcon 3EC direct electron detector in counting mode, and representative 2D class averages. **b)** Angular distribution of projections. **c)** Gold-standard Fourier shell correlation for the reconstruction of the full complex or the polymerase component after focussed refinement, and resolution estimation using the 0.143 criterion. **d)** Cryo-EM maps of the full complex (left) and polymerase component after focussed refinement (right) color-coded by local resolution.
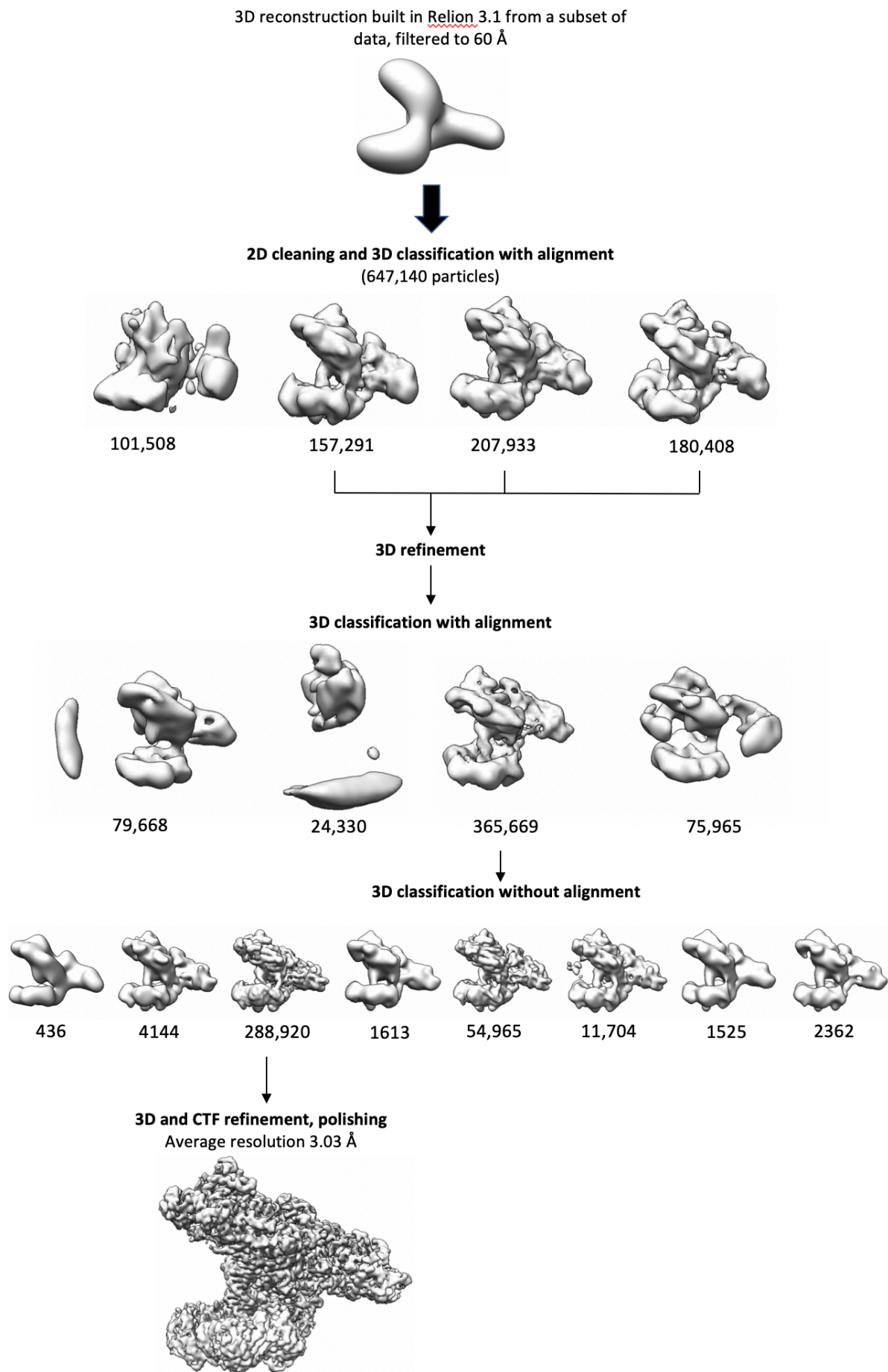
Supplementary Figure 2. Overview of image processing of Pol δ holoenzyme with different PCNA conformers (Dataset 1).

Supplementary Figure 3. Sample separation of the Pol δ-DNA-PCNA-FEN1 complex. **a)** Gel filtration chromatography of the reconstituted Pol δ-DNA-PCNA-FEN1 complex. **b)** The numbered peak fractions in a) were analysed by SDS-PAGE (lanes 1–7). Proteins corresponding to the bands are labeled on the right. Molecular weight standards are shown on the left.

Supplementary Figure 4. Cryo-EM of the processive Pol δ holoenzyme (Dataset 2). **a)** Electron micrograph (aligned sum) acquired on a K3 direct electron detector in super resolution mode, and representative 2D class averages. **b)** Angular distribution of projections. **c)** Gold-standard Fourier shell correlation for the complex, and resolution estimation using the 0.143 criterion. **d)** Cryo-EM map of the complex, color-coded by local resolution.

Supplementary Figure 5. Overview of image processing of the processive Pol δ holoenzyme (Dataset 2). No alternative conformers of PCNA were observed in this data set compared to that shown in Supplementary Figures 1 and 2.
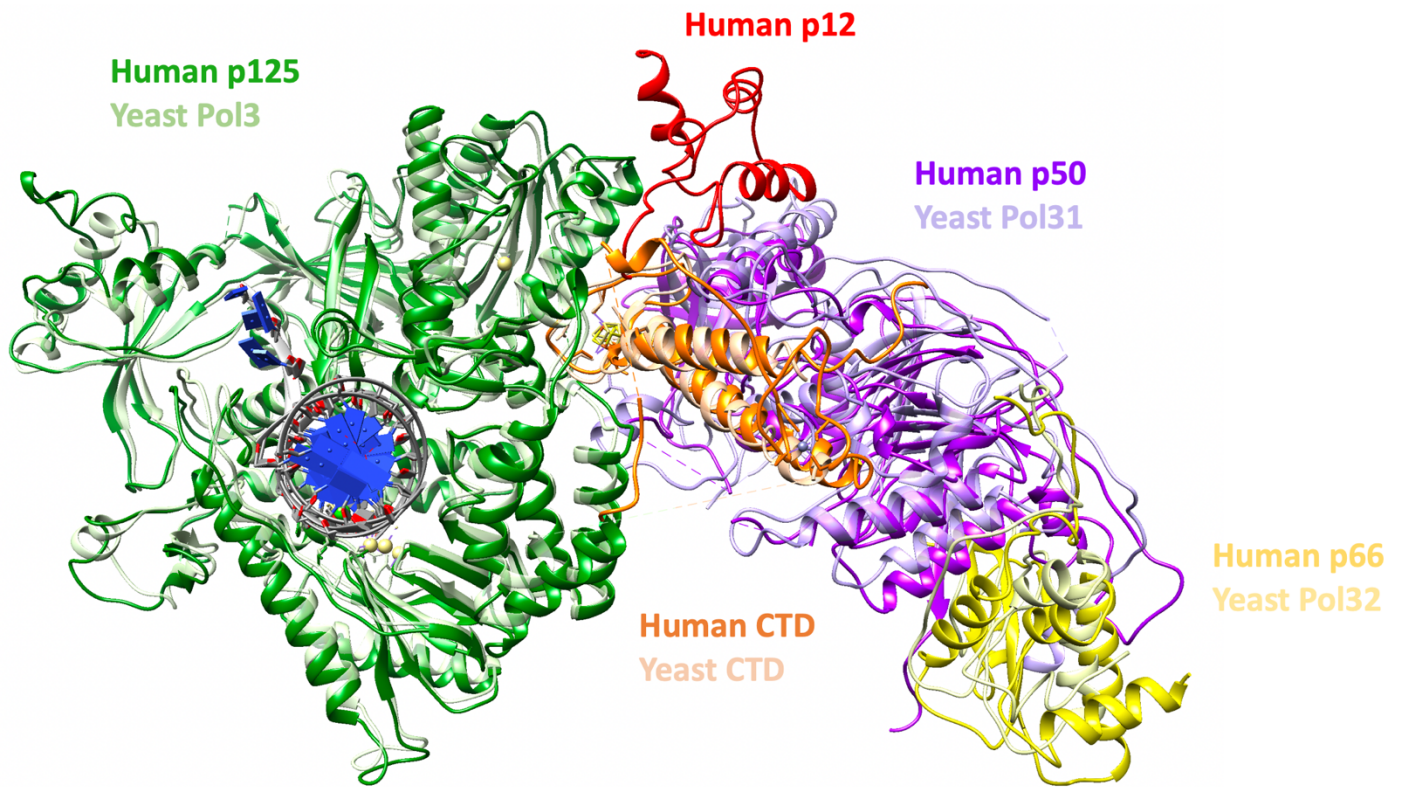
Supplementary Figure 6. Processive human Pol δ holoenzyme overlaid with the *S. cerevisiae* homologue (PDB: 6P1H). For clarity, PCNA was removed from the processive Pol δ holoenzyme structure.
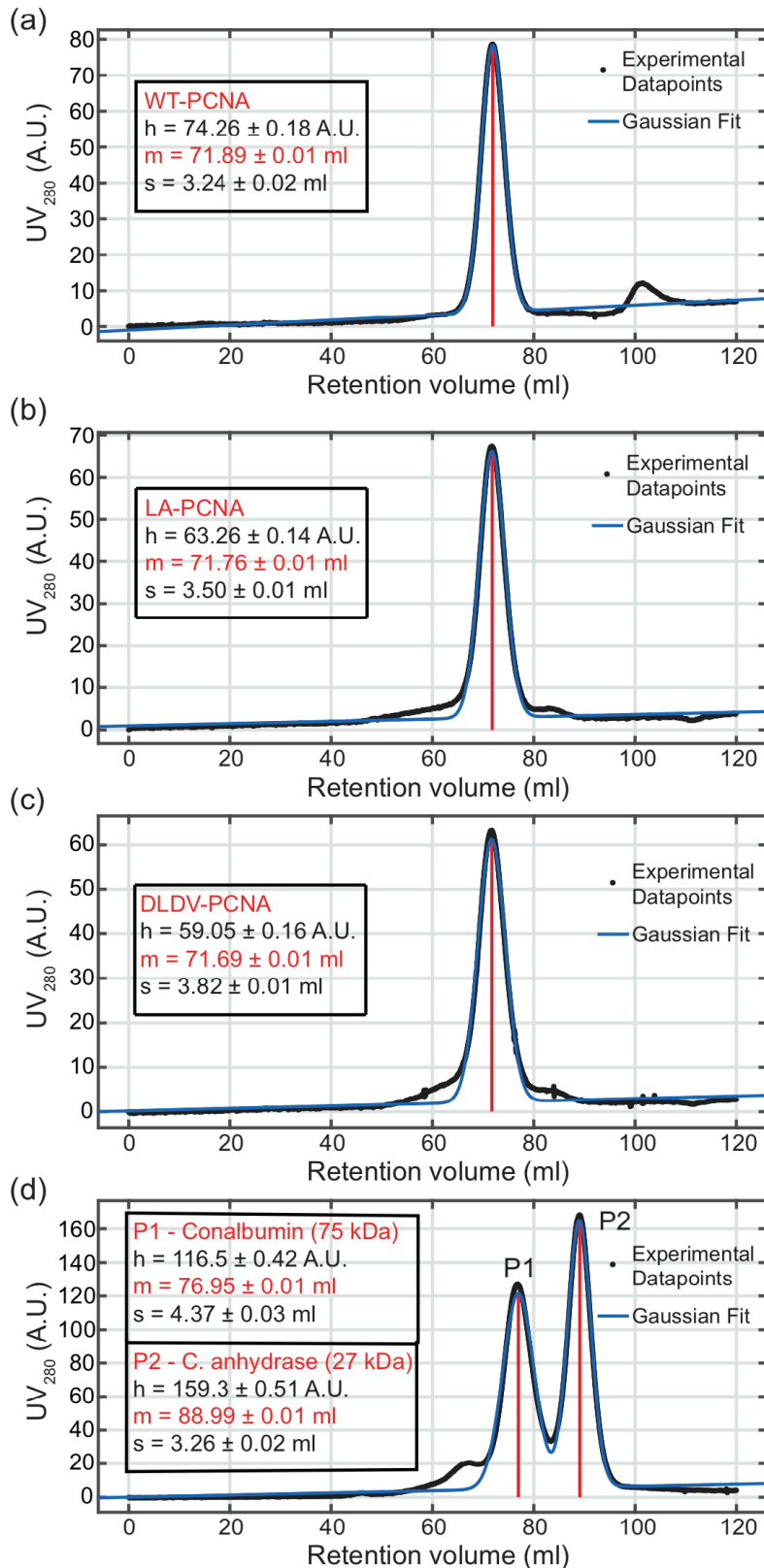
Supplementary Figure 7. Gel filtration profiles of WT-PCNA and mutants PCNA. The fitted elution profiles are shown for the following proteins: **a)** WT-PCNA, **b)** LA-PCNA, **c)** DLDV-PCNA, **d)** Molecular weight markers Carbonic anhydrase (27 kDa) and Conalbumin (75 kDa). Fittings of the elution peaks of the purified WT-PCNA and mutant PCNAs and comparison to the elution of molecular markers. The values of the Gaussian fitting parameters are recorded in the inset tables together with their 95% confidence interval. The vertical red lines represent the positions of the maxima of the elution peaks.
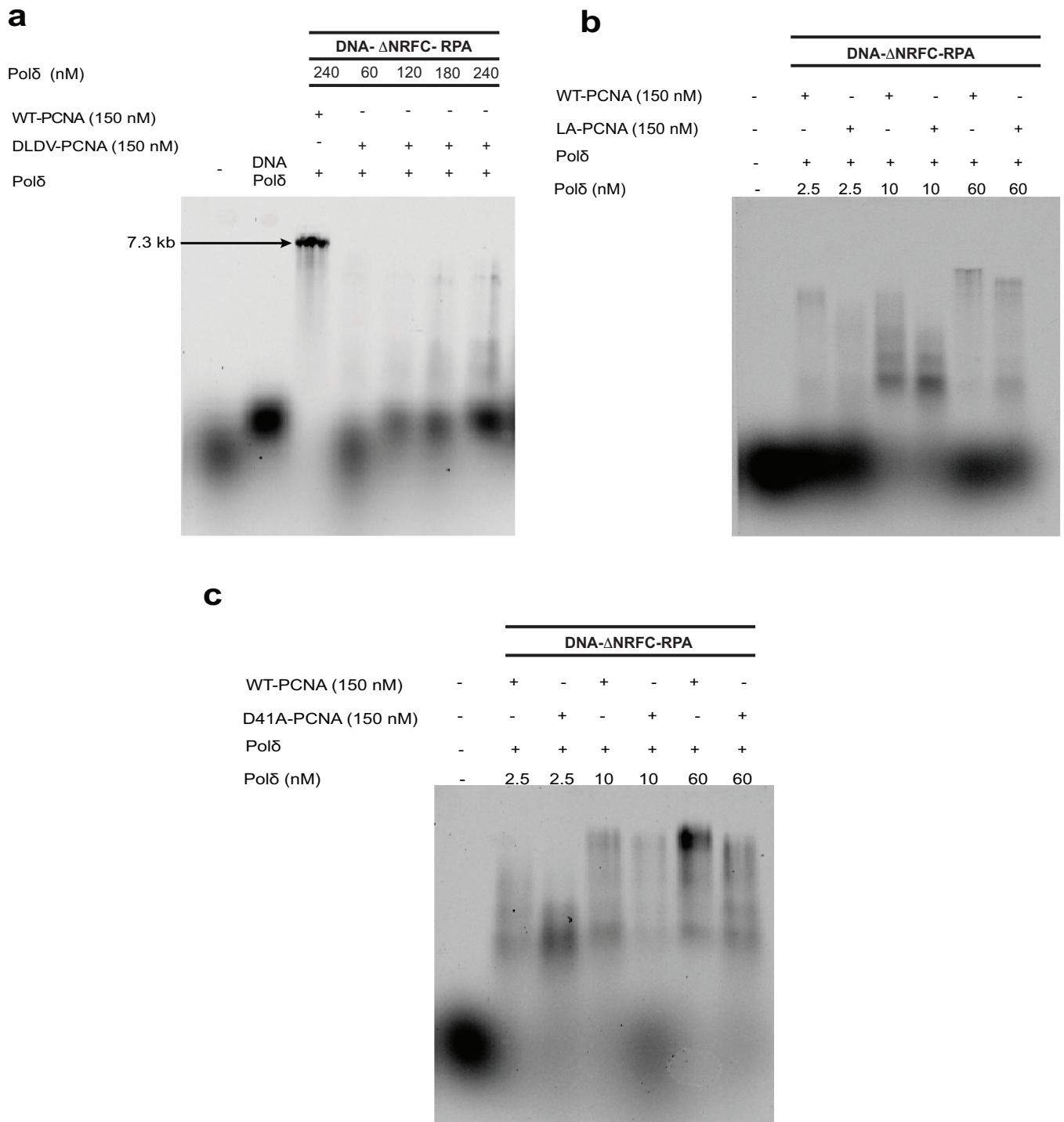
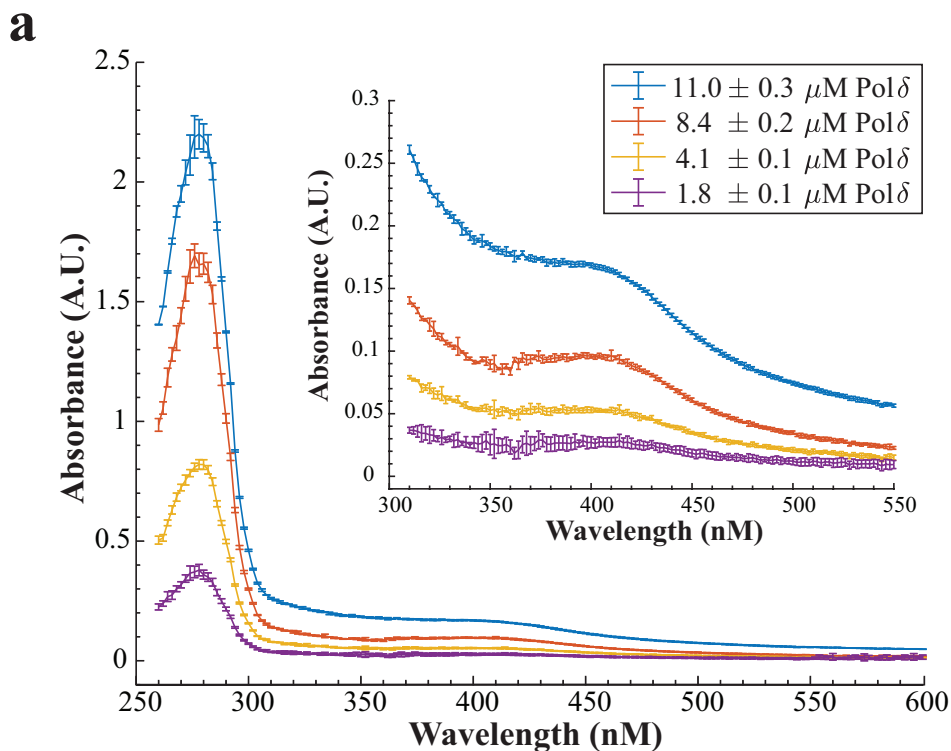**Supplementary Figure 8.** Primer extension assays with Pol δ and PCNA mutants. **a)** M13mp18 DNA primer extension assay with different concentrations of Pol δ using DLDV-PCNA mutant. Reactions were carried out at 30 °C for 10 min. **b)** M13mp18 DNA primer extension assay with different concentrations of Pol δ using LA-PCNA mutant. Reactions were carried out at 30 °C for 2.5 min. **c)** M13mp18 DNA primer extension assay with different concentrations of Pol δ using D41A-PCNA mutant. Reactions were carried out at 30 °C for 2.30 min. Products were separated on 1% alkaline agarose gel at 10 V for 20 hrs.
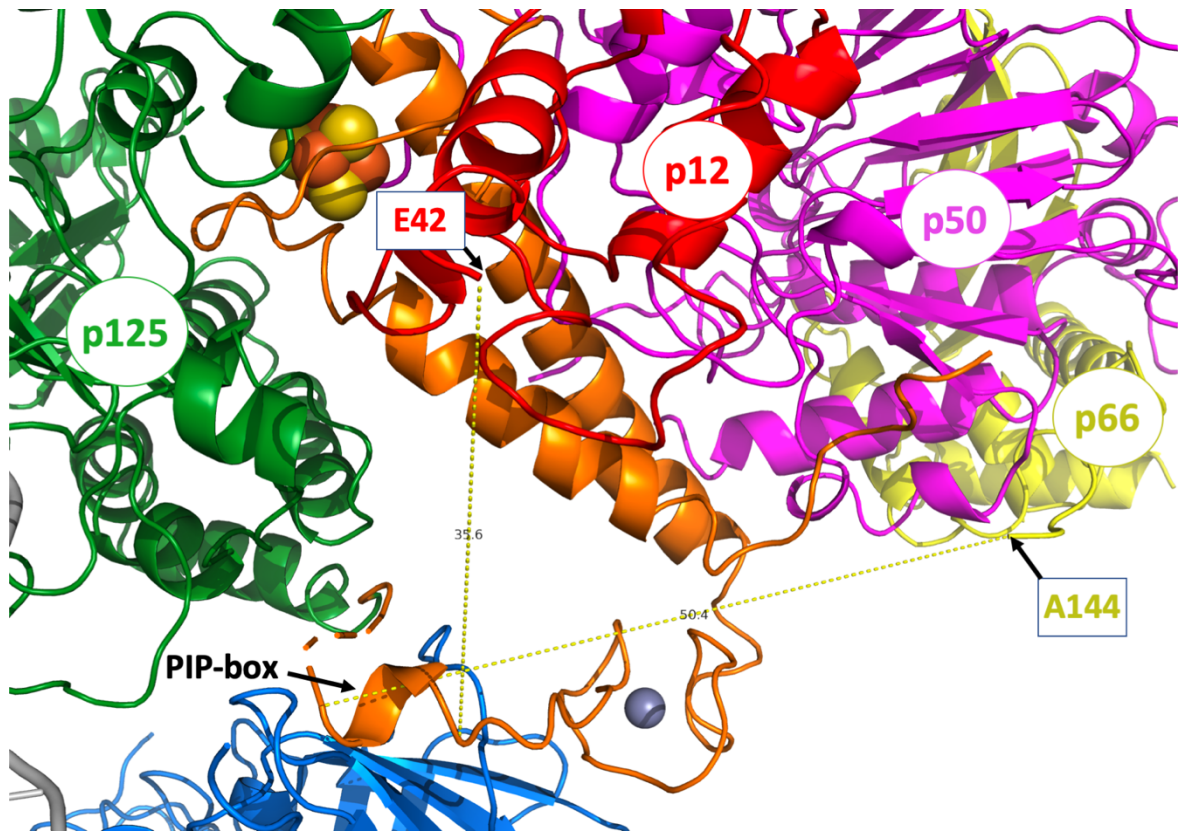
Supplementary Figure 9. Distance between the last visible residue of p66 (A144, 308 residues from the p66 PIP-box) and the N-terminus of the CTD PIP-box is ~50 Å. The distance between the first visible residue of p12 (E42, 31 residues from the p12 PIP-box) and the C-terminus of the PIP-box is ~36 Å.
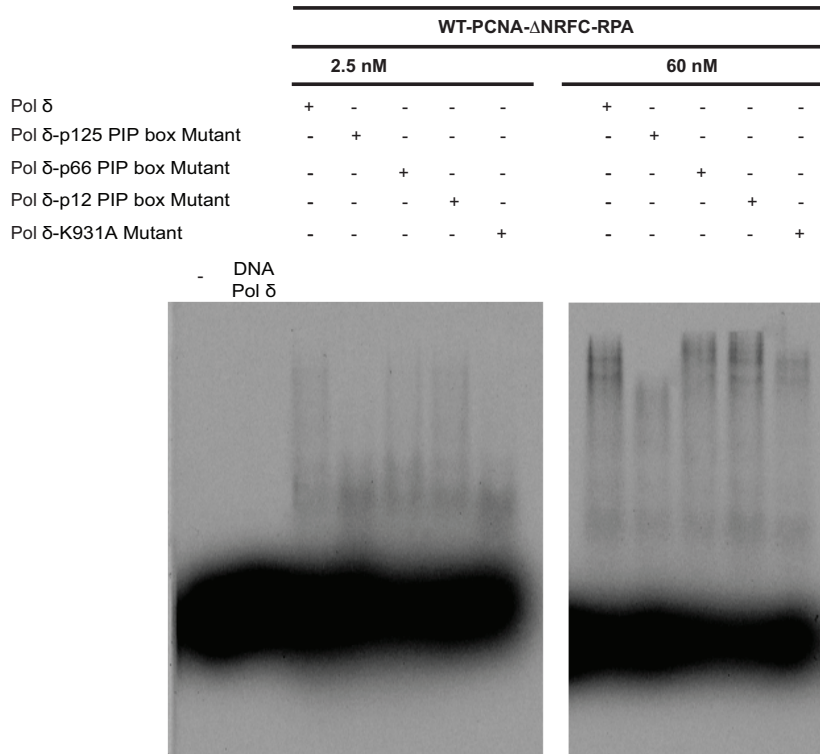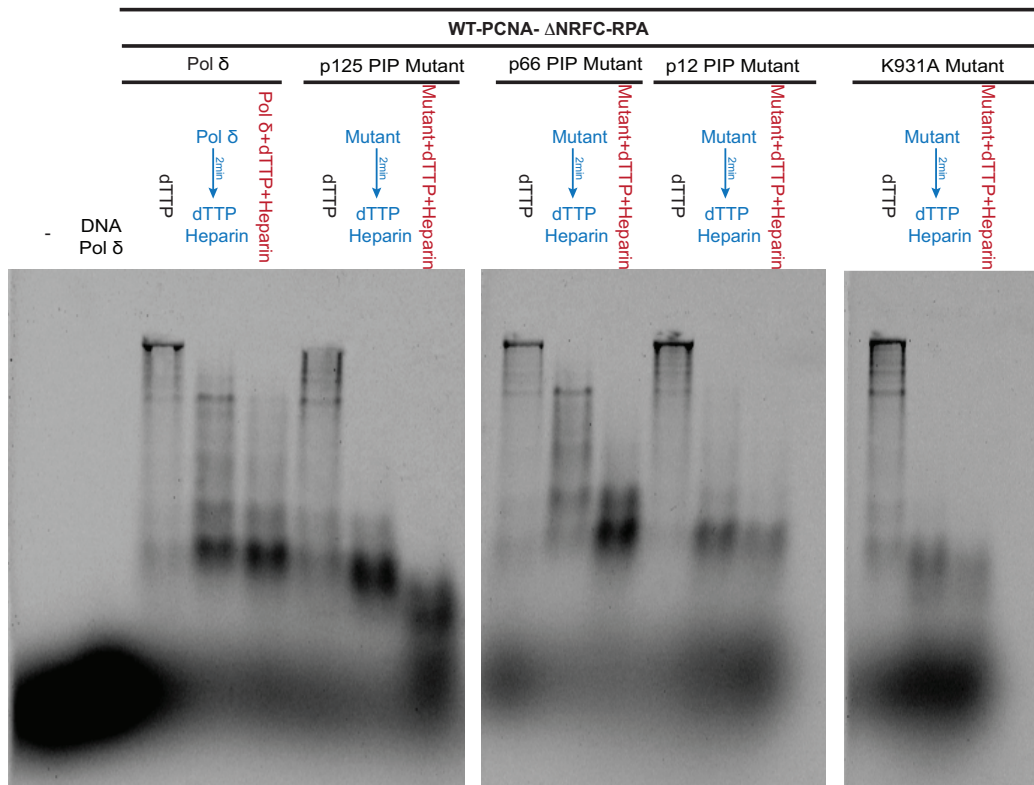
Supplementary Figure 10. Primer extension and processivity assays with Pol δ and Pol δ mutants. **a)** M13mp18 DNA primer extension assay with different concentrations of Pol δ, Pol δ-p125 PIP box mutant, Pol δ-p66 PIP box mutant, Pol δ-p12 PIP box mutant and Pol δ-K931A mutant as indicated. Reactions were carried out at 30 °C for 2.30 min. **b)** Processivity of Pol δ, Pol δ-p125 PIP box mutant, Pol δ-p66 PIP box mutant, Pol δ-p12 PIP box mutant and Pol δ-K931A mutant with or without 575 ng/ml heparin. Reactions were initiated with 500 μM dTTP with or without heparin. All reactions were carried out at 30 °C for 5 min and products were separated on 1% alkaline agarose gel at 10 V for 20 hrs.

a

b

|	Repeat	Pol δ Concentration (μM)			
		11.0 ± 0.3	**8.4 ± 0.2**	**4.1 ± 0.1**	**1.8 ± 0.1**
A_{280} (A.U.)	1	2.2347	1.6241	0.7995	0.3447
	2	2.1299	1.6975	0.8297	0.3754
	3	2.2351	1.6169	0.8057	0.3421
	4	2.137	1.6994	0.8429	0.3763
A_{410} (A.U.)	1	0.1633	0.0963	0.0558	0.0327
	2	0.1624	0.0937	0.0526	0.0249
	3	0.1661	0.1024	0.0513	0.0257
	4	0.1652	0.0934	0.0522	0.0253
$\varepsilon_{410}=\varepsilon_{280}*A_{410}/A_{280}$ ($M^{-1}cm^{-1}$)	1	14479.02	11748.59	13828.91	18796.57
	2	15107.72	10937.09	12561.36	13142.48
	3	14724.64	12548.42	12615.84	14885.12
	4	15317.14	10922.02	12270.62	13321.66

Supplementary Figure 11. Characterization of the FeS cluster in Pol δ. **a**) UV-Vis absorption spectra in the region 260-600 nm of Pol δ at four concentrations. The spectra show a broad absorption band which has a peak at ~410 nm that scales with the Pol δ concentration. The inset shows a zoomed-in view of the spectra that focuses on the 410 nm broad absorption band. The spectra were acquired as described in the Methods section. Each data point in each spectrum represents the average of four measurements. The error bars represent the standard deviation (SD) of the four measurements. **b)** Absorbance measurements and calculations of Pol δ extinction coefficient at 410 nm and the average number of iron atoms per protein. Values are calculated as described in Methods section from four measurements per each Pol δ concentration. Mean ε_{410}= 13575.45 ± 1980.83 $M^{-1}.cm^{-1}$ and [Fe]/[Pol δ] = 3.4 ± 0.5.
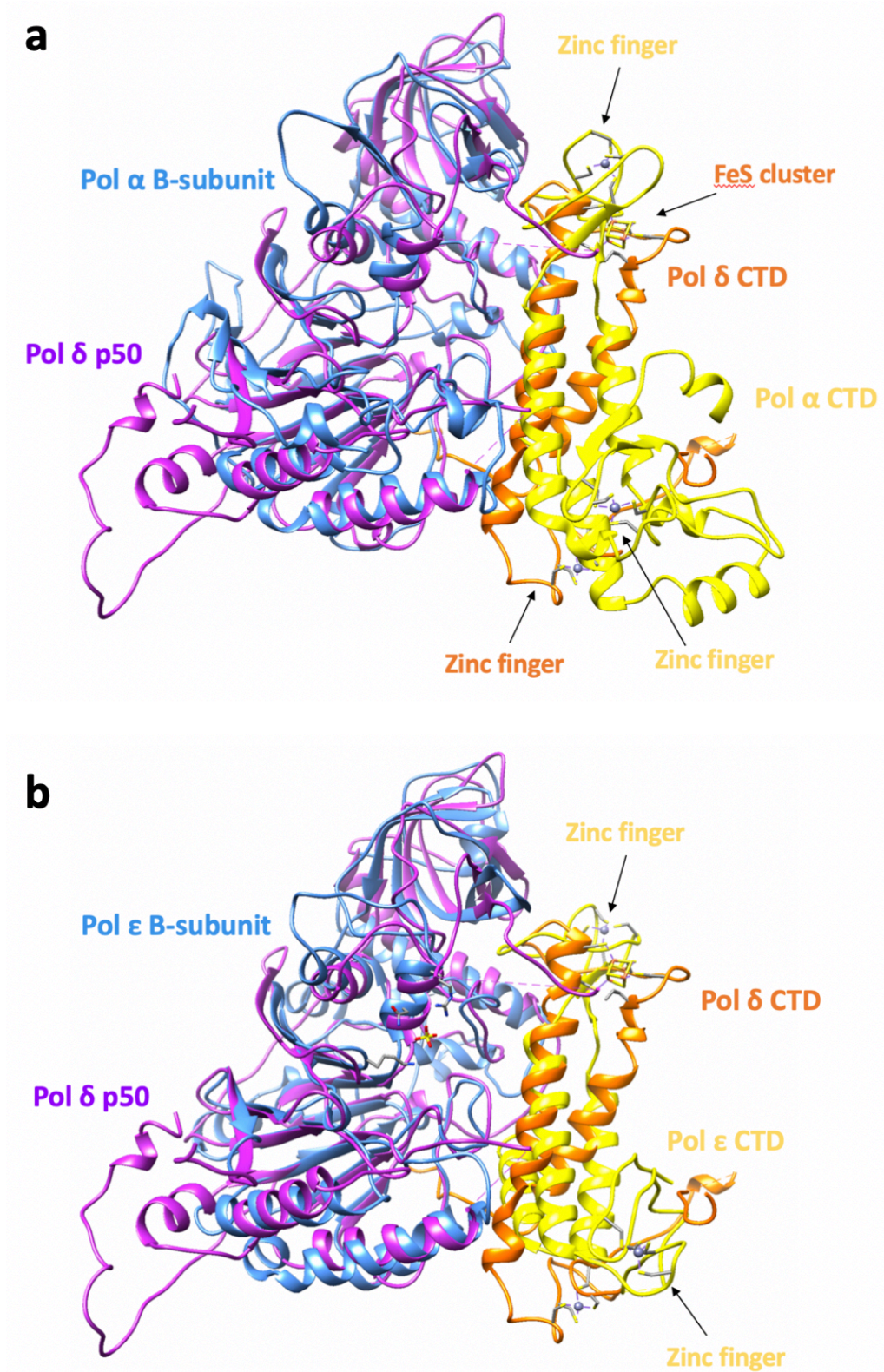
Supplementary Figure 12. Orientation of the CTD relative to the B-subunit in Pol δ, α and ε. a) Comparison of the B-subunit–CTD complex of Pol δ with Pol α. b) Comparison of the B-subunit–CTD complex of Pol δ with Pol ε. The cryo-EM model of Pol δ was aligned to that of Pol α (PDB entry 4Y97) or Pol ε (PDB entry 5VBN) using the B-subunit. The metal binding sites in the CTDs are labelled. Models are shown in ribbon representation. Zinc ion and Fe-S centre are shown as a sphere and cube, respectively.
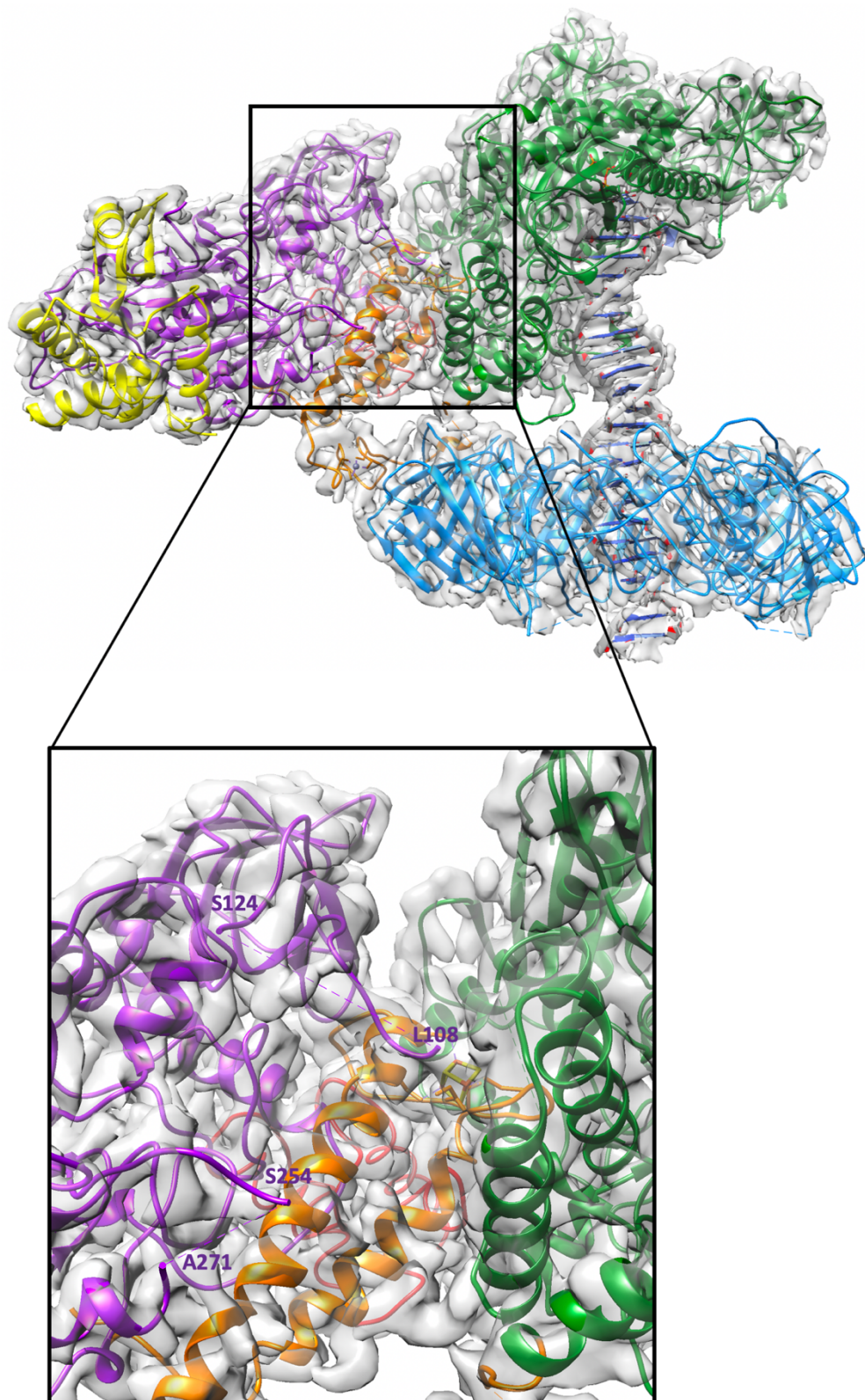
Supplementary Figure 13. Inset (bottom) from the model of the processive holoenzyme (top) showing the unmodeled loops of p50 (255-270 and 109-123) which face the catalytic subunit.
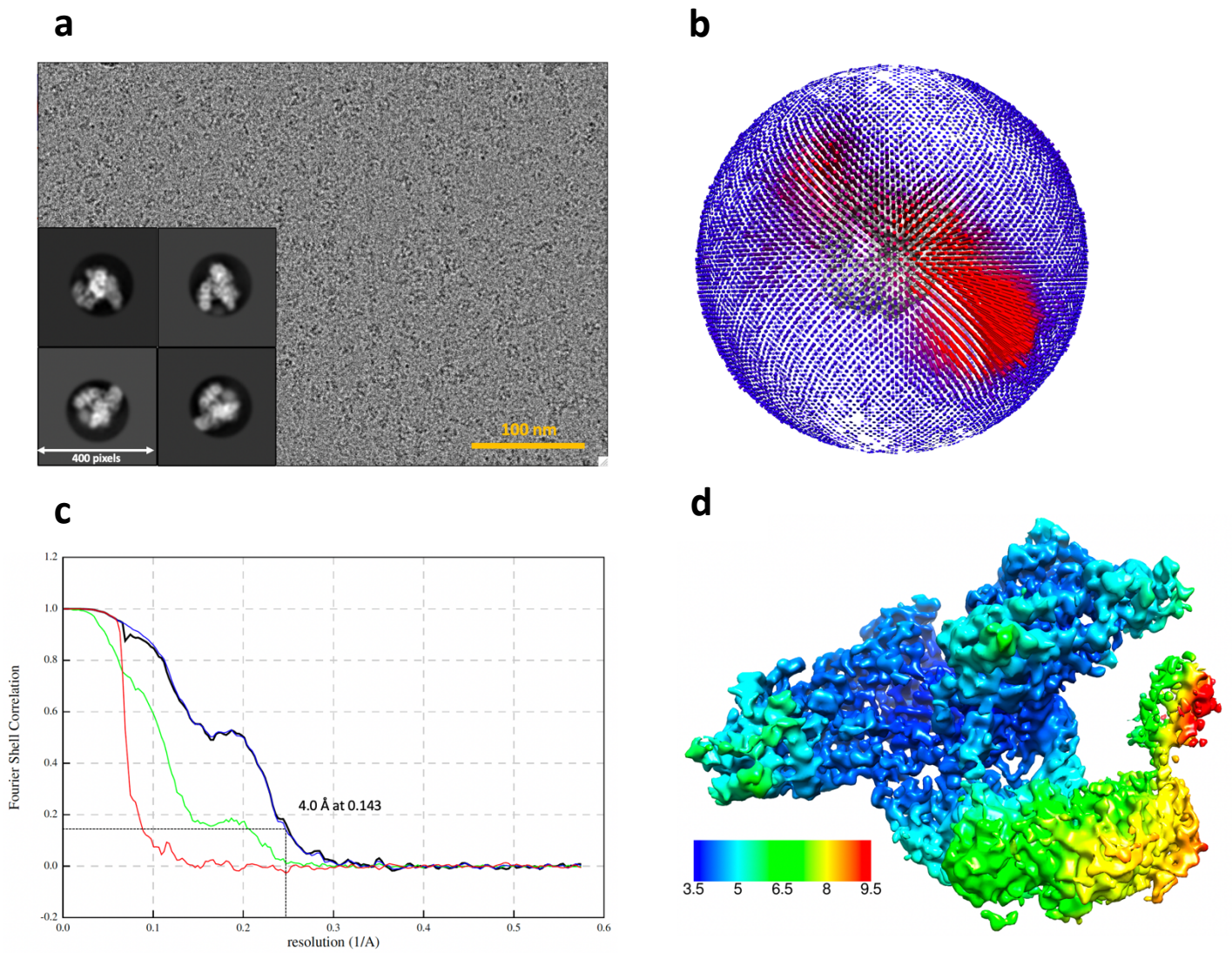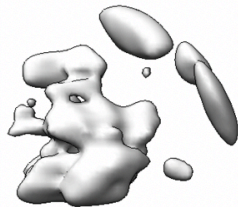
Supplementary Figure 14. Cryo-EM of the Pol δ-DNA-PCNA-FEN1 toolbelt complex. **a)** Electron micrograph (aligned sum) acquired on a K3 direct electron detector in super resolution mode, and representative 2D class averages. **b)** Angular distribution of projections. **c)** Gold-standard Fourier shell correlation for the complex, and resolution estimation using the 0.143 criterion. **d)** Cryo-EM map of the complex, color-coded by local resolution.
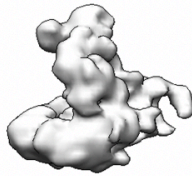
3D reconstruction of the same complex previously generated
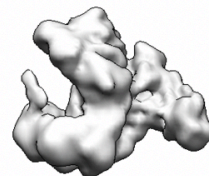in Relion 3.0, filtered to 30 Å
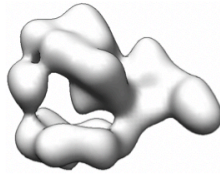
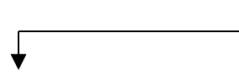**2D cleaning and 3D classification with alignment**
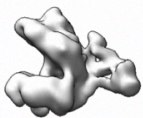(866,036 particles)

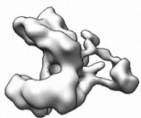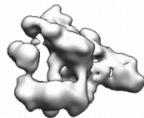185,246   329,483   351,307
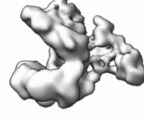
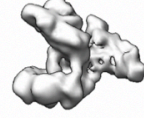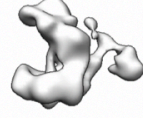**3D classification with alignment**

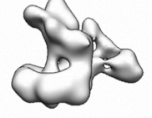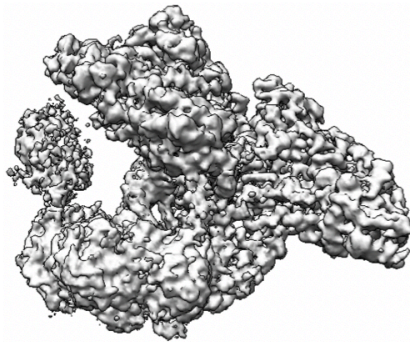31,498   41,300   23,305   47,291   89,631   71,337   22,787   24,158

3D and CTF refinement, polishing
Average resolution 4.0 Å

Supplementary Figure 15. Overview of image processing of the Pol δ-DNA-PCNA-FEN1 complex.

Supplementary Table 1 | Cryo-EM data collection, refinement and validation statistics

	Processive Polδ-DNA-PCNA complex (EMD- 10539) (PDB 6TNY)	Polδ-DNA-PCNA-FEN1 complex (EMDB-10540) (PDB 6TNZ)	Polδ-DNA-PCNA complex Conformer 1 (EMDB- 10080) (PDB 6S1M)	Polδ-DNA-PCNA complex Conformer 2 (EMDB- 10081) (PDB 6S1N)	Polδ-DNA-PCNA complex Conformer 3 (EMDB- 10082) (PDB 6S1O)
Data collection and processing					
Magnification	105,000	105,000	75,000	75,000	75,000
Voltage (kV)	300	300	300	300	300
Electron exposure (e–/Å^2)	44	44	35	35	35
Defocus range (μm)	-1.1 to -2.3	-1.1 to -2.3	-0.4 to -0.6	-0.4 to -0.6	-0.4 to -0.6
Pixel size (Å)	0.87	0.87	1.08	1.08	1.08
Symmetry imposed	C1	C1	C1	C1	C1
Initial particle images (no.)	2,512,757	2,512,757	2,821,297	2,821,297	2,821,297
Final particle images (no.)	288,920	47,291	96,612	32,282	8571
Map resolution (Å)	3.03	4.05	4.27	4.86	8.10
FSC threshold	0.143	0.143	0.143	0.143	0.143
Map resolution range (Å)	2.84-15.5	3.68-10.0	4.02-10.7	4.42-15.4	9.19-24.4
Refinement					
Initial model used (PDB code)					
Model resolution (Å)	3.03	4.05	4.27	4.86	8.10
FSC threshold	0.143	0.143	0.143	0.143	0.143
Model resolution range (Å)	2.84-15.5	3.68-10.0	4.02-10.7	4.42-15.4	9.19-24.4
Map sharpening B factor (Å^2)	-5.32	6.05	5.64	7.45	6.18
Model composition					
Non-hydrogen atoms	19,728	22,010	19728	19728	19728
Protein residues	2399	2705	2399	2399	2399
Nucleotide residues	50	50	50	50	50
Ligands	3	3	3	3	3
B factors (Å^2)					
Protein	63.41	65.03	50.28		
Nucleotide	149.74	149.74	163.98		
Ligand	31.02	31.02	31.02		
R.m.s. deviations					
Bond lengths (Å)	0.007	0.007	0.008	0.009	0.009
Bond angles (°)	1.093	1.130	1.215	1.322	1.312
Validation					
MolProbity score	1.87	2.31	2.24	2.35	2.30
Clashscore	7.94	13.59	13.13	14.59	14.59
Poor rotamers (%)	0.83	1.57	1.46	1.96	1.70
Ramachandran plot					
Favored (%)	93.24	91.08	91.93	92.75	92.79
Allowed (%)	6.42	7.84	7.22	6.72	6.68
Disallowed (%)	0.34	1.09	0.84	0.53	0.53